Structure Development of a Polybutadiene/Polyisoprene Blend during Spinodal Decomposition. Comparison between Light Scattering and Optical Microscopy

Jörg Läuger,† Rainer Lay, Swen Maas, and Wolfram Gronski*

Institut für Makromolekulare Chemie und Freiburger Materialforschungszentrum, Universität Freiburg, Stefan-Meier-Strasse 31, 79104 Freiburg, FRG

Received February 24, 1995; Revised Manuscript Received July 11, 1995®

ABSTRACT: The typical interconnected bicontinuous percolation structure of a critical 50/50 wt % polybutadiene (PB)/polyisoprene (PI) mixture was characterized in detail by the structure function of a light scattering experiment and by statistical image processing of optical microscope images. The time development of the interdomain distance and the local radius of the curved interface in the late stage of the spinodal decomposition are obtained for the first time for the same system by both methods and are found to be in good agreement. PB/PI blends are systems with a lower critical solution temperature (LCST). The critical point was varied within a wide temperature range by changing the 1,2 content of the PB. For optical microscopy, the structure was fixed by photo-cross-linking and the optical contrast was achieved in a second step by selective staining of the PI phase by exposing the sample to iodine vapor.

Introduction

The understanding of the phase separation dynamics in binary polymer mixtures is important not only from a purely scientific viewpoint but also for many practical applications. The long chain molecules of polymeric systems lead to long diffusion times and make such blends useful as ideal systems for experimental observations of phase separation dynamics.[1] On the other hand the parameters of the constituent polymers can be changed to alter the morphology and therefore the physical properties of the mixture in a way not possible in one-component materials.[2] One important mechanism of a phase separation process is the spinodal decomposition (SD). Therefore the understanding of the SD process is of great interest and a large number of publications reflects the importance of this type of phase separation. Nevertheless the knowledge of SD is far from being complete and there are many open questions. A good overview on the topic is given by Hashimoto in a recent review article.[3]

In a previous publication we described light scattering and light microscopy experiments of an off-critical PB/PI blend where we observed a so-called percolation-to-cluster transition with both methods.[4] The aim of this paper is the study of SD of a critical polymer mixture. It is the first time, to our knowledge, that a quantitative determination of structure quantities was carried out in both real and reciprocal space for the same polymer blend.

The process of SD can be separated into at least three different stages, the so-called early, intermediate, and late stages, each having a characteristic time dependence of the concentration fluctuations.[5,6] In the early stage the fluctuations grow exponentially and the dynamics can be described by the linear Cahn theory.[7] The scattering vector of the dominant fluctuation mode $q_m(t)$ observed as a maximum of the intensity distribution (spinodal ring) is related to the interdomain distance $L_m(t)$ by the equation

$$L_m(t) = 2\pi/q_m(t) \tag{1}$$

In the early stage q_m stays constant and only the composition of the phases changes. In the intermediate stage, $q_m(t)$ decreases because of structure growth. In the late stage the compositions of the phases reach the final composition while $q_m(t)$ continues to decrease. The driving force of the decomposition process and the structure growth in this stage is the interface tension, which tends to reduce the total interface area, leading to a smoother interface between the two phases.

In the intermediate and the late stages of SD the time evolution of the intensity $I_m(t)$ and the position of the scattering maximum $q_m(t)$ are described by power laws:

$$I_m(t) \propto t^{\beta} \qquad q_m(t) \propto t^{-\alpha} \tag{2}$$

In the intermediate stage the relation $\beta > 3\alpha$ holds, whereas in the late stage the equation $\beta = 3\alpha$ is valid.[8] The latter relation represents the universality of the structure function in the late stage of SD. The structure function is defined as[9]

$$F(x) = q_m^3(t)\, Ix(t) \qquad \text{with} \qquad x(t) = q/q_m(t) \tag{3}$$

Besides the interdomain distance, a second structure property, the local curvature radius of the interface, is accessible by the structure function. According to Tomita, $F(x)$ for a two-phase system with a smooth interface, as is the case in the late stages of a SD process, can be approximated by[10]

$$I(q) \propto q^{-4}(1 + q^{-2})/R_m^2 + \ldots \tag{4}$$

$R_m(t)$ represents the mean radius of the curved interface and is illustrated in Figure 1 together with the interdomain distance $L_m(t)$.

The first term in (4) corresponds to the Porod law, which is dominant for a very smooth interface, i.e., when $R_m(t)$ is large.[11] In the case of small q values the structure function decreases with a q^{-6} behavior, i.e. more rapidly than in the Porod law regime. The

* To whom correspondence should be sent.
† Present address: Department of Chemical Engineering, Stanford University, Stanford, CA 94305.
® Abstract published in *Advance ACS Abstracts,* September 1, 1995.

0024-9297/95/2228-7010$09.00/0

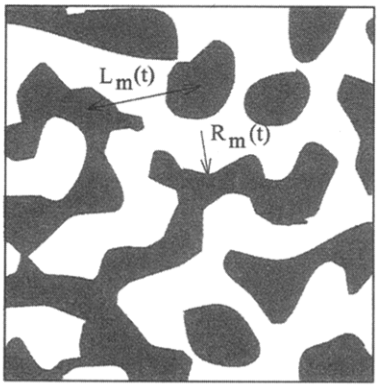

Figure 1. Schematic illustration of the interdomain distance and the radius of the local interface curvature of the bicontinuous percolation structure typical for spinodal decomposition.

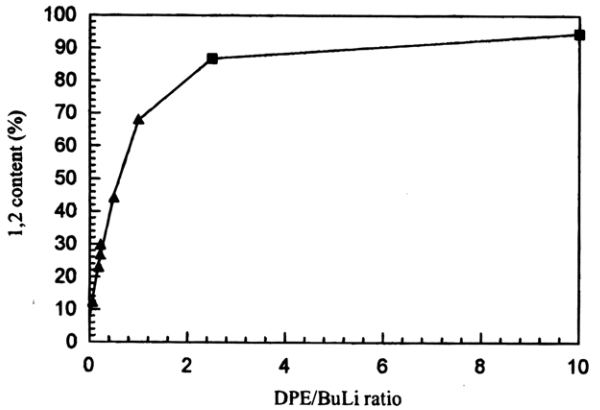

Figure 2. 1,2 content of PB as a function of the DPE/BuLi ratio at 50 °C in cyclohexane as solvent: (▲) our experiments; (■) data from Halasa et al.[12]

crossover scattering vector from the q^{-6} behavior to the Porod regime is predicted by Tomita's theory:[10]

$$q_c(t) = 1/R_m(t) \tag{5}$$

With the crossover value in the normalized structure function representation $x_c = q_c(t)/q_m(t)$ this leads to

$$R_m(t) = 1/x_c q_m(t) \tag{6}$$

For that reason it is possible to obtain the average local curvature radius of the interface from the position of the crossover to the Porod region.

Experimental Section

1. Samples. Polybutadiene (PB) and polyisoprene (PI) were polymerized in a pressure vessel by living anionic polymerization. The synthesis was performed with *sec*-butyllithium (BuLi) as initiator and cyclohexane as solvent at 20 and 50 °C, respectively. The 1,2 content of PB was controlled by the ratio BuLi/dipiperidinoethane (DPE).[12] Figure 2 shows the influence of the DPE concentration on the 1,2 content of PB particularly in the range up to a DPE/BuLi ratio of 1. The solid line in Figure 2 connects the values of our experiments and the data published by Halasa et al.[12]

The molecular weights were determined by membrane osmometry and gel permeation chromatography (GPC) in toluene with a RI detector. For correction of M_n in GPC we used the molecular weight determined by osmotic measurements in toluene. The molecular weights and the molecular weight distributions of the polymers as well as the 1,2 content of the PB polymers determined by ^{1}H NMR are summarized in Table 1. According to ^{13}C NMR the ratio of cis to trans is about 2/3 for all PB samples and both PI polymers have a content of 77 mol % cis, 18 mol % trans, and 5 mol % 3,4 units.

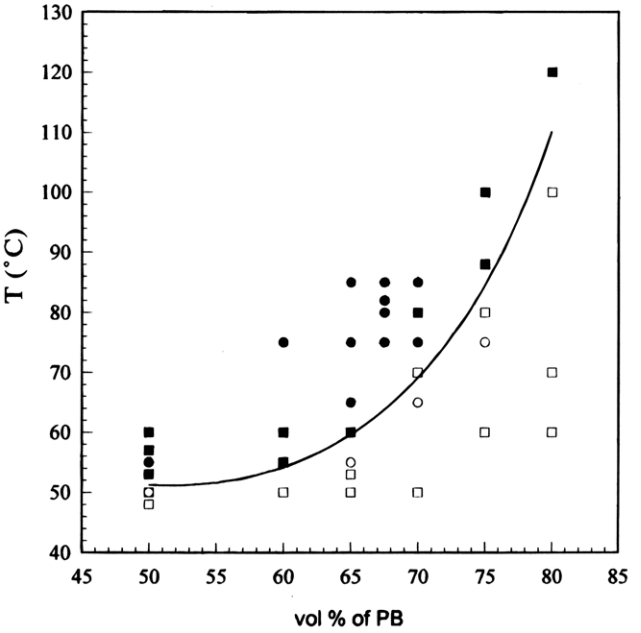

Figure 3. Phase diagram determined by DSC (squares) and SALS (circles) for the PB110/PI5 blend: (open symbols) one-phase region; (closed symbols) two-phase region.

Table 1. Properties of the Polybutadiene (PB) and Polyisoprene (PI) Polymers

polymer	M_n (GPC)	M_n (osmotic pressure)	M_W/M_n	1,2 content of PB (mol %)
PB 102	159 000	151 000	1.2	23.8
PB 103	106 000		1.09	17.3
PB 110	97 000	109 000	1.07	23.0
PB 111	101 000		1.08	26.8
PI 5	105 000	112 000	1.08	
PI 6	98 000	100 000	1.12	

The blends were prepared by precipitation from 10 wt % toluene solutions in methanol, and the precipitated blends were dried under vacuum for 1 week. 1,4-PI and 1,4-PB have different thermal expansion coefficients.[13] This leads to a positive *excess* free energy[13,14] and a negative *excess* volume[14] of mixing and thus to phase separation with a lower critical solution temperature (LCST).[13,14] Because 1,4-PI and 1,2-PB have the same expansion coefficients, the LCST of PB/1,4-PI blends increases with the 1,2 content of PB.[13] In order to obtain phase diagrams DSC measurements were performed with a Perkin-Elmer DSC 7. The blends were annealed between 2 and 12 h at a certain temperature, followed by quenching in liquid N_2. The heat capacity changes were recorded during reheating 25 mg samples at a heating rate of 40 deg/min from −120 to 0 °C. One or two glass transition temperatures (T_g) were obtained in the DSC curves, depending on the blend composition and the annealing temperature. The phase transition temperatures were determined by the crossover to the double T_g behavior. The precision to which the phase diagrams are determined is clarified in Figure 3 for experiments with the blend PB110/PI5 used in the following optical experiments.

In addition to the DSC results also data points from light scattering experiments are shown. A smooth curve was added to separate the homogeneous region from the two-phase region. The phase diagrams determined by DSC of four different blends of the polymers listed in Table 1 are given in Figure 4.

For the cases of the polymers having nearly the same molecular weight the phase diagrams were obtained by symmetrizing curves of the type shown in Figure 3. For the unsymmetrical blend PB102/PI5 the measurements were carried out over the whole composition range. The blend PB110/PI5 having a LCST of 52 °C was used in the SD experiments described below.

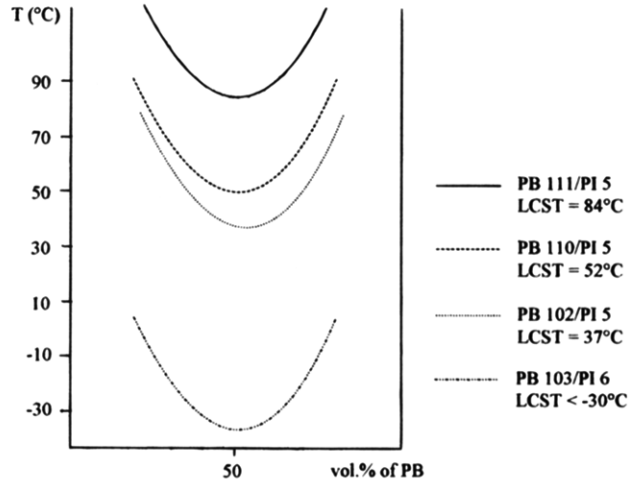

Figure 4. Phase diagrams determined by DSC of four different PB/PI blends of the polymers listed in Table 1.

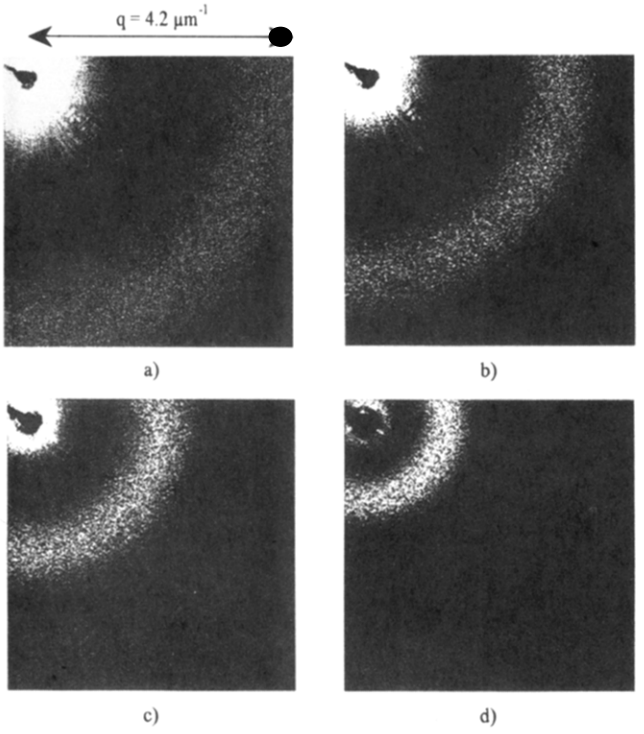

Figure 5. SALS patterns of a critical PB110/PI5 mixture at a temperature of 75 °C and after 30 (a), 40 (b), 60 (c), and 100 (d) min of demixing.

2. Small Angle Light Scattering (SALS). The SALS device is part of a combined Rheo-SALS apparatus and has been described in full detail elsewhere.[15] Here we only want to mention the parts relevant to the present study. The light source is a 10 mW linear polarized He−Ne laser with a wavelength of 633 nm. The incident light was attenuated by an appropriate neutral density filter. After this filter a rotating ground plate removes a speckle pattern due to interferences at static refractive index inhomogeneities in the sample. Otherwise the speckle pattern is superimposed on the scattering pattern.[16] The sample was placed into a heating chamber between two quartz plates separated by a spacer of 0.5 mm. The temperature is controlled within a temperature range from 20 to 220 °C with an accuracy of ±0.2 deg. The incident beam in the sample was focused to a diameter of 0.8 mm. The scattered light intensity distribution $I(q)$ was determined using a two-dimensional CCD detector with 512 × 512 pixels, each with an area of 19 × 19 μm. The scattered light was focused directly on the active area of the detector by a focusing optical system. The unscattered incident light beam was directed onto a beam stopper in one corner of the CCD camera. With this layout we are able to detect one quarter of the scattering pattern in a scattering vector range from 0.5 to 4.2 μm^{-1}. The scattering vector is related to the scattering angle θ and the wavelength λ of the laser in the sample:

$$q = (4\pi/\lambda) \sin(\theta/2) \quad (7)$$

The direct focusing of the scattered light onto the detector allows a quantitative analysis of the intensity distributions. Circular integration of the circular symmetric patterns yields smooth intensity distributions from which the structure functions are obtained at a very good signal to noise ratio.

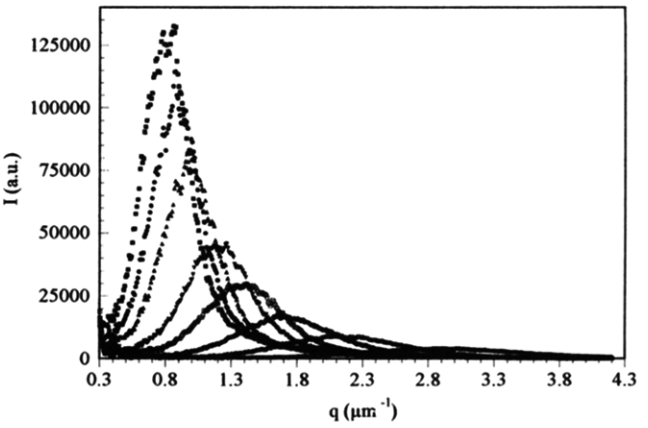

Figure 6. Raw data of the intensity distributions of the PB110/PI5 blend at different times after the temperature jump in the two-phase region at 75 °C: (▽) 30 min; (△) 40 min; (○) 50 min; (□) 62 min; (▼) 72 min; (▲) 88 min; (●) 98 min; (■) 108 min.

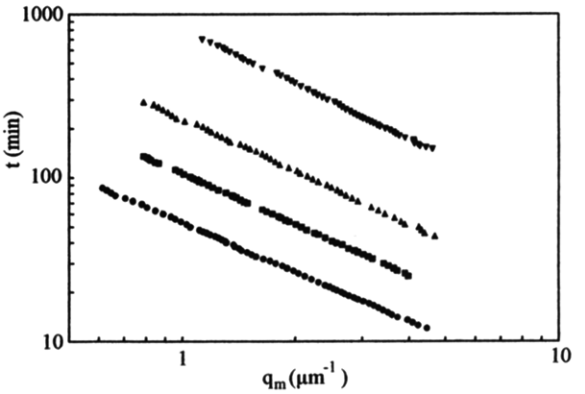

Figure 7. Temperature dependence of the spinodal decomposition process (top to bottom): (▼) 55 °C; (▲) 65 °C; (■) 75 °C; (●) 85 °C.

3. Optical Microscopy. Samples for microscopy were prepared by casting from 10 wt % solution in toluene after drying in vacuum for 3 days. The resulting 30−40 μm thin films were annealed at the same temperature as for the SALS experiment. After different annealing times the morphology of the samples was fixed by photo-cross-linking. The cross-linking agent was 1,12-dodecamethylenebis(maleimide) contained in the blend at a concentration of 2.0−3.0 wt %. The photo-cross-linking was done by irradiation by UV light from a mercury lamp (λ_{max} = 360 nm) for 20 min. Subsequently, the contrast for LM was achieved by selectively staining the polyisoprene phase by exposing the films to iodine vapor for 20 min.[17] The fixed and stained films were mounted in a microscope (Olympus AH2). The optical photographs were digitized by scanning into a computer. After passing through a low-pass filter, they were converted into binary images to improve the contrast. For the setting of the threshold gray value the compositions of the phases are assumed to consist of pure PB and PI, respectively. Therefore, for the case of critical mixtures of polymers with nearly equal molecular weights the resulting binary images consist of white (PB) and

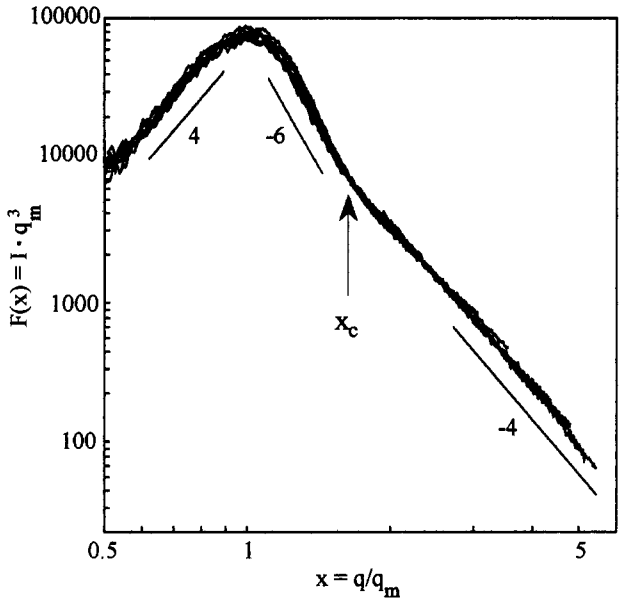

Figure 8. Structure function representation of the intensity distributions of Figure 6 according to eq 3.

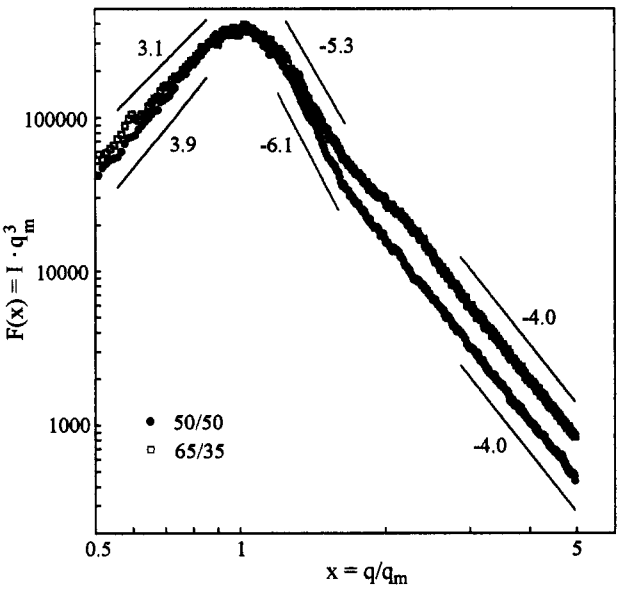

Figure 9. Structure functions of the critical (50/50) and one off-critical (65/35) mixture after a demixing time of 65 min at 85 °C.

black (PI) regions of equal area. The structure properties are obtained by processing the binary images by the IBAS software (Kontron Co.), as discussed in the following.

Results and Discussion

1. SALS Experiments. Figure 5 shows SALS patterns 30, 40, 60, and 90 min after a temperature jump from room temperature to the two-phase region at 75 °C. During the SD the spinodal ring contracts toward the beam center and increases in intensity.

The intensity distributions $I(q)$ after various demixing times are shown in Figure 6.

In a previous publication we showed for the same sample that the position q_m and the intensity I_m at the maximum of the distribution follow a power law behavior according to eq 2.[15] The ratio β/α of the exponents in eq 2 is 2.9. Therefore, the system is definitely in the late stage of SD at the selected temperature and in the observed q range.

With the use of eq 1 it is possible to obtain the time dependence of the interdomain distance (L_m) from the time dependence of the scattering vector at the maximum (q_m).

In Figure 7 the temperature dependence of the SD process is shown: Increasing temperature, i.e. deeper quenches, yields smaller q_m values at the same decomposition time which means a faster coarsening of the structure.

In a representation with reduced time and scattering vector quantities, a scaling of the curves in Figure 7 on one single curve is possible.[18,19] For such a procedure the temperature dependent characteristic scattering vector $q_m(t=0,T)$ and effective diffusion constant $D_{eff}(T)$ have to be determined from the early stage of SD which is not observable within the limited q range of our SALS apparatus.

According to eq 6 the local curvature radius of the interface is obtained from the universal structure function. Figure 8 shows the universal structure function constructed on the basis of eq 3 from the intensity distributions for the different demixing times shown in Figure 6.

According to Figure 8 one can distinguish three regions where different power laws are valid:

$$F(x) \propto \begin{cases} x^4 & x < 1 \\ x^{-6} & 1 < x < 1.8 \\ x^{-4} & x > 1.8 \end{cases} \quad (8)$$

The crossover between the x^{-6} regime to the Porod x^{-4} scattering is precisely defined in the experimental curve to be $x_c = 1.8$. In the small x regime ($x < x_c$) the structure function can be approximated by a theoretical function proposed by Furukawa for deep quenches of critical mixtures where a self-similar bicontinuous percolation structure exists:[20,21]

$$F(x) = \frac{x^4}{3/2 + x^{10}} \quad (9)$$

The x^{-6} behavior is in agreement with other experiments on different systems.[5,8,22-24] For $x < 1$ the x^4 dependence is in agreement with some theoretical[20,25] and experimental results.[24,26] A possible reason for the disagreement with a few experimental results[5,8,22,23] may be that the x^4 dependence is valid only in the late stage of the SD of a critical mixture if significant thermal force contributions are absent. Takenaka and Hashimoto[24] showed for PB/SBR blends that a x^3 dependence is valid at higher temperatures, whereas the x^4 dependence fits their structure function better at lower temperatures.

Besides the measurements at the critical composition of the PB/PI blends, we investigated the SD of off-critical mixtures. A detailed description of a so-called pinning effect and a percolation–cluster transition (PCT) in such a mixture is given elsewhere.[4] Here we only want to discuss a structure function of an off-critical mixture where no pinning and no percolation-to-cluster transition was observed and $q_m(t)$ and $I_m(t)$ show the same power law behavior as the critical mixture. This function shows a behavior different from the structure function of the critical mixture. In Figure 9 the structure functions are plotted for the case of the critical (50/50) and an off-critical (65/35) mixture at 85 °C and after 65 min of SD.

The curves are scaled to the same intensity at the maximum. At higher x values again the Porod law is

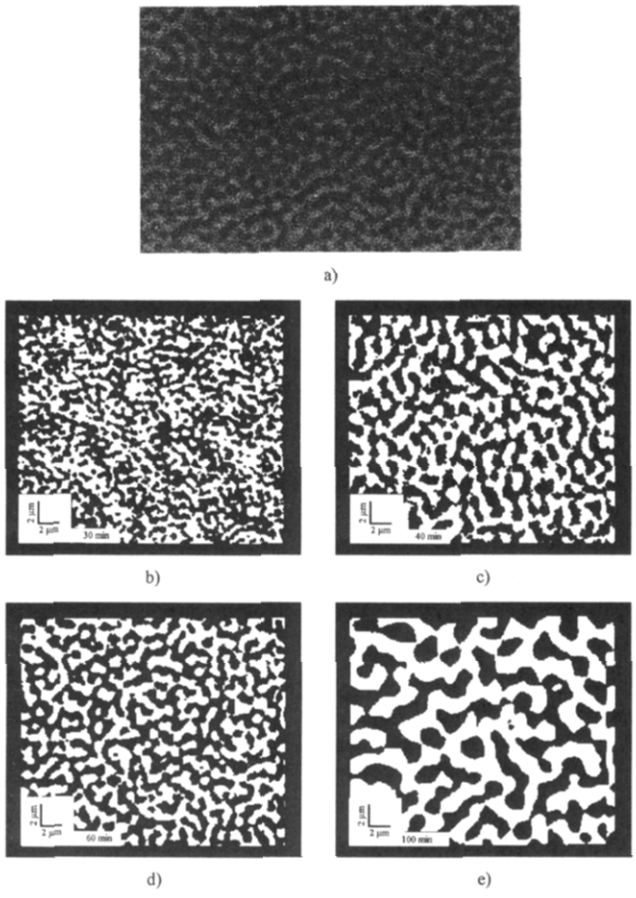

Figure 10. LM pictures: (a) original photograph after 100 min; (b)–(e) binary images after demixing times of 30, 40, 60, and 100 min.

valid in both cases. At smaller x values there are differences between the two compositions: First the slopes in the range $x < 1$ and $1 < x < 1.8$ are lower for the off-critical mixture, being +3.1 and −5.3, respectively, instead of +4 and −6 for the critical mixture. In fact the structure function is broadened considerably after the PCT has occurred.[26] Therefore the smaller slopes near the maximum in the case of the off-critical mixture probably indicate the onset of the disruption of the domains as a prestage of the PCT. Second, the structure function of the off-critical mixture has a higher order maximum at $x = 2$, which is suppressed in the critical mixture. This indicates a local lamellar structure due to a smooth interface. It has been shown that the second-order peak of the structure function of lamellar systems is suppressed when the volume fraction is $\phi = 1/2$.[3] In our experimental structure function we did not see a higher order peak, which is expected for the critical mixture to occur at $x = 3$.

2. Light Microscopy Experiments. As a result of the described microscopy method Figure 10 shows binary images of the films annealed at 75 °C after different demixing periods. Additionally, a photograph after an annealing time of 100 min is shown.

Comparison between this photograph and the binary images shows that the digitizing and binarizing process leaves the structure unaltered in its essential features. Therefore a true reproduction of the expected bicontinuous percolation structure is obtained with our technique, keeping in mind that the images are two-dimensional cross sections of a three-dimensional percolation structure. Therefore, the structure changes of the PB/PI blend during SD can be visualized also in real space.

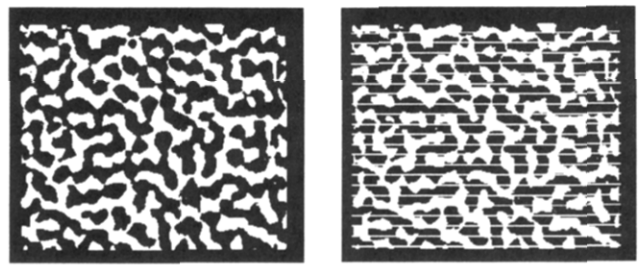

Figure 11. Example for the determination of the interdomain distance (see text).

Table 2. Comparison of SALS and LM Results for the Interdomain Distance and the Average Local Radius of the Curved Interface

	interdomain distance (μm)		local curvature radius (μm)	
demixing time (min)	SALS (±0.1)	LM (±0.5)	SALS (±0.05)	LM (±0.15)
33	2.0	2.3	0.18	
40	2.5	3.1	0.23	
50	3.0	3.3	0.27	
60	3.6	3.7	0.33	0.44
90	5.3	5.3	0.48	0.52
100	5.7	5.9	0.54	0.61
135	7.9	7.5	0.72	0.73

The procedure of determining the interdomain distance is depicted in Figure 11.

By digital imaging processing, it is possible to measure the mean size of the black or the white regions. For this purpose a set of equidistant lines was superimposed on the picture. The distance between the lines was taken as the estimated thickness of the percolation structure. The average of the sizes of black or white sections was determined from a distribution of about 300 sections. In our case of a 50/50 wt % mixture of polymers with nearly equal molecular weights the mean interdomain distance is 2 times the mean size of the regions. Table 2 lists the interdomain distances for different demixing times obtained with SALS and LM. It is seen that there is a good conformity between the results of the two methods.

With the image processing procedure the local radius of the curved interface R_m can also be determined from the microscopy images. The procedure is illustrated in Figure 12.

In a first step the course of the interface was extracted from the binary image (Figure 12a) by digital image analysis (Figure 12b). The sections of greatest curvature were selected manually by setting marks (Figure 12c). The image analyzing software then calculates the radius of a circle from the end points of the selected sections and the height of the arcs. An average was obtained from more than 100 curved sections for each demixing time. Table 2 also compares the R_m values obtained by SALS and LM after different demixing times. Because of the smaller structures and the limited resolution of the microscopy images the comparison is restricted to longer demixing times, i.e. to larger structures. For the curvature radius as well as for the interdomain distance a good agreement between the values obtained from the two different optical methods is achieved considering the fact that the radius is near the resolution limit of the optical microscope for smaller demixing times.

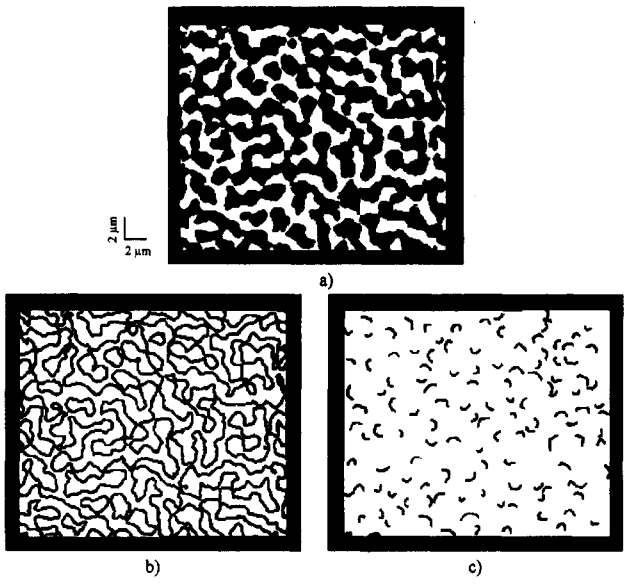

Figure 12. Determination of the local radius of the curved interface from LM pictures and digital image processing: (a) binary image; (b) course of the interface; (c) local curvatures of the interface.

Conclusion

It has been shown that the structure development of PB/PI blends during spinodal decomposition can be observed in the reciprocal space of the light scattering experiment as well as in real space with optical microscopy. From a quantitative analysis of the structure function the time dependence of structure parameters such as the interdomain distance and the local radius of the curved interface is obtained. With image processing methods the interdomain distance and the local radius of the curved interface obtained from the microscope patterns were in agreement with the corresponding values determined from light scattering. First, this demonstrates that reliable results are also obtained by the specially devised staining technique used for optical imaging. Second, it supports the interpretation of the crossover in the q dependence of the structure function in terms of the curvature radius of the interface. The underlying model can now be applied with greater confidence in future applications to similar problems.

Acknowledgment. Financial support by the Freiburger Materialforschungszentrum and the Deutsche Forschungsgemeinschaft through the Sonderforschungsbereich 60 and the Graduiertenkolleg "Strukturbildung in Makromolekularen Systemen" is gratefully acknowledged.

References and Notes

(1) Hashimoto, T. In *Current Topics in Polymer Science*; Ottenbrite, R. M., Utracki, L. A., Inoue, S., Eds.; Hanser: München, 1987; Vol. II. *Phase Transitions* **1988**, *12*, 47.
(2) *Polymer Blends*; Paul, D. R., Newman, S., Eds.; Academic: New York, 1978; Vols. I + II.
(3) Hashimoto, T. In *Materials Science and Technology*; Cahn, R. W., Haasen, P., Kramer, E. J., Eds.; VCH: Weinheim, New York, 1993; Vol. 12.
(4) Läuger, J.; Lay, R.; Gronski, W. *J. Chem. Phys.* **1994**, *101*, 7181.
(5) Bates, F. S.; Wiltzius, P. *J. Chem. Phys.* **1989**, *91*, 3258.
(6) Hashimoto, T.; Takenaka, M.; Jinnai, H. *J. Appl. Crystallogr.* **1991**, *24*, 457.
(7) Cahn, J. W. *J. Chem. Phys.* **1965**, *42*, 93.
(8) Hashimoto, T.; Itakura, M.; Hasegawa, H. *J. Chem. Phys.* **1986**, *85*, 6118.
(9) Binder, K.; Stauffer, D. *Phys. Rev. Lett.* **1974**, *33*, 1006.
(10) Tomita, H. *Prog. Theor. Phys.* **1984**, *72*, 656.
(11) Porod, G. *Kolloid-Z* **1952**, *125*, 108.
(12) Halasa, A. F.; Lohr, D.; Hall, J. *J. Polym. Sci., Polym. Chem.* **1981**, *19*, 1357.
(13) Task, C. A.; Roland, C. M. *Polym. Commun.* **1988**, *29*, 332.
(14) Kawahara, S.; Sato, K.; Akiyama, S. *J. Polym. Sci., Polym. Phys.* **1994**, *32*, 15.
(15) Läuger, J.; Gronski, W. *Rheol. Acta* **1995**, *34*, 70.
(16) Bates, F. S.; Dierker, S. B.; Wignall, G. D. *Macromolecules* **1986**, *19*, 1938.
(17) Thakur, M. *Macromolecules* **1988**, *21*, 661.
(18) Kedrowski, C.; Bates, F. S.; Wiltzius, P. *Macromolecules* **1993**, *26*, 3448.
(19) Izumiani, T.; Takenaka, M.; Hashimoto, T. *J. Chem. Phys.* **1990**, *92*, 3213.
(20) Furukawa, H. *J. Phys. Soc. Jpn.* **1989**, *58*, 216.
(21) Furukawa, H. *Phys. Rev. B* **1989**, *40*, 2341.
(22) Tomlins, P. E.; Higgins, J. S. *J. Chem. Phys.* **1989**, *90*, 6691.
(23) Hashimoto, T.; Takenaka, M.; Izumitani, T. *Polym. Commun.* **1989**, *30*, 45.
(24) Takenaka, M.; Hashimoto, T. *J. Chem. Phys.* **1992**, *96*, 6177.
(25) Yueng, C. *Phys. Rev. Lett.* **1988**, *61*, 1135.
(26) Takenaka, M.; Izumitani, T.; Hashimoto, T. *J. Chem. Phys.* **1993**, *98*, 3528.

MA950237T